# Role of deep levels and interface states in the capacitance characteristics of all-sputtered $CuInSe_2/CdS$ solar cell heterojunctions

J. Santamaria, G. Gonzalez Diaz, E Iborra, I. Martil, and F. Sanchez-Quesada
*Departamento Electricidad y Electronica, Facultad de Ciencias Fisicas, Universidad Complutense, 28040 Madrid, Spain*

(Received 9 August 1988; accepted for publication 30 November 1988)

All-sputtered $CuInSe_2/CdS$ solar cell heterojunctions have been analyzed by means of capacitance-frequency ($C$-$F$) and capacitance-bias voltage ($C$-$V$) measurements. Depending on the $CuInSe_2$ layer composition, two kinds of heterojunctions were analyzed: type 1 heterojunctions (based on stoichiometric or slightly In-rich $CuInSe_2$ layers) and type 2 heterojunctions (based on Cu-rich $CuInSe_2$ layers). In type 1 heterojunctions, a 80-meV donor level has been found. Densities of interface states in the range $10^{10}$–$10^{11}$ $cm^2\,eV^{-1}$ (type 1) and in the range $10^{12}$–$10^{13}$ $cm^{-2}\,eV^{-1}$ (type 2) have been deduced. On the other hand, doping concentrations of $1.6\times10^{16}$ $cm^{-3}$ for stoichiometric $CuInSe_2$ (type 1 heterojunction) and $8\times10^{17}$ $cm^{-3}$ for the CdS (type 2 heterojunction) have been deduced from $C$-$V$ measurements.

## I. INTRODUCTION

Thin-film $CuInSe_2/CdS$ heterojunctions have been a subject of considerable interest in recent years due to their potential use for terrestrial photovoltaic applications. Much effort has been devoted to analyze and model the operation mechanisms of such structures. Time dependent, intensity of illumination dependent, and several other effects have been reported,[1,2] which suggest that device efficiency could be limited by deep levels in the semiconductors or by interface states. Interface states are due to lattice mismatch, impurities, grain boundaries, electron bombardment in sputtered devices, etc., while deep levels are usually related to stoichiometric defects in the semiconductors. Many studies have been reported about the existence and influence of interface states[3,4] and deep levels[5,6] on evaporated devices which, up to date, have shown the highest efficiency. Nevertheless, to our knowledge, less work has been done on sputtered cells. Sputtered cells, despite their considerably lower efficiency, are of interest because the potential offered by the technique for low cost, large-scale production of solar cells.

In this paper, we present a study of capacitance measurements on all sputtered $CuInSe_2/CdS$ heterojunctions. Capacitance versus frequency characteristics at variable temperature and at various dc bias voltages are used to obtain information about deep levels and interface states.[7]

## II. EXPERIMENT

### A. Sample preparation

All-sputtered $CuInSe_2/CdS$ heterojunctions were grown in a GCA Vacuum Industries apparatus described elsewhere.[8] The growth process was as follows:

Alumina substrates, chemically cleaned, were coated with a 0.1–0.2-$\mu$m rf sputtered molybdenum layer. Thin films (2–3 $\mu$m) of $CuInSe_2$ were then deposited by sputtering a Se excess target in $Ar/H_2$ atomospheres at a substrate temperature varying between 350 and 450 °C. At 350 °C, stoichiometric or slightly In-rich chalcopyrite films were obtained with resistivities of about 750 Ω cm and a mobility of 0.5 $cm^2/V$ s. At higher growth temperatures, Cu-rich samples were obtained with resistivities in the range 10–$10^{-1}$ Ω cm.[9] CdS thin films (2 $\mu$m) were then sputtered with a resistivity of 2 Ω cm and a mobility of 3.5 $cm^2/V$ s, measured on additional test substrates.[8]

Two kinds of heterojunctions will be studied: type 1 heterojunctions produced with stoichiometric $CuInSe_2$, which showed the following photovoltaic parameters: $J_{sc} = 22$ $mA/cm^2$, $V_{oc} = 0.277$ V, FF = 0.34; and type 2 heterojunctions, produced with Cu-rich $CuInSe_2$, which presented a vanishingly low photovoltaic response.[10]

### B. Heterojunction characterization

Heterojunction characterization was done as follows: Complex impedance at frequencies in the range 100 Hz–10 MHz and at dc bias voltages from −0.8 to 0.5 V were measured with a 4192-A Hewelett-Packard impedance analyzer. The dc signal was measured directly on the device with a Keithley 195-A digital multimeter which was automatically disconnected just before the impedance measurement in order to avoid perturbations due to the input impedance of the voltmeter. All of the systems were controlled with a HP-86 computer through an IEEE-488 bus.

The sample was mounted in a holder which could be cooled down to liquid nitrogen temperature and warmed up to 570 K. The measurement temperature was varied between 220 and 340 K.

In the following, we will show results of a representative heterojunction of each type. These results are representative of a set of 20 analyzed heterojunctions.

## III. RESULTS AND DISCUSSION

### A. $C$-$F$ measurements

It is well known that the admittance of a $p$-$n$ junction is frequency dependent. Neglecting the effect of free carriers that will respond in the high-frequency scale, the frequency dispersion of the admittance at intermediate or low frequency can be attributed to deep levels in the bulk semiconduc-

 0021-8979/89/083236-06$02.40  

tors or to interface states. Changes in the occupancy of deep levels and interface states at the point where they cross the Fermi level result in a new contribution to the capacitance, which relaxes at characteristic frequencies above which carriers at those states cannot follow the ac signal. A peak in conductance or losses is observed at those frequencies. In the following, we will show that *C-F* measurements, performed at variable temperature, can be very useful in determining the energetic position of deep levels. Also, *C-F* measurements at several forward dc biases are a very powerful tool in determining relative interface state distributions.[11]

### 1. Type 1 heterojunction

Figure 1 shows the frequency dispersion of capacitance and losses of the representative type 1 heterojunction (made with near stoichiometric or slightly In-rich $CuInSe_2$) at 300 K. Measurements were taken at 0 dc bias, although qualitative similar results were obtained with reverse bias voltages in the range 0–1 V. In order to eliminate the influence of series and shunt resistances on data, these were corrected according to the model proposed by Chopra and Das.[12]

A relaxation in the $10^5$ Hz range can be observed. A shift in the position of this relaxation was observed when the temperature was varied in the range 220–340 K. Following the theory of admittance spectroscopy,[7] the characteristic frequency of the relaxation process can be related to the energetic position of the trap according to the following equation:

$$\omega = N_B v_{\rm th} \sigma \exp(-\Delta E/kT), \qquad (1)$$

where $\sigma$ is the capture cross section, $v_{\rm th}$ is the thermal velocity, and $N_B$ is the effective density of states in the band of $CuInSe_2$. In principle, the position of the trap can be determined, providing the temperature dependence of the preexponential factor is known. The $T^2$ dependence of the product $N_B v_{\rm th}$ is usually taken into account, but the temperature dependence of the capture cross section is often unknown, although, in some cases, an experimental dependence in the form $T^{-N}$ has been observed.[13,14] We have taken $N = 2$ according to results quoted in Refs. 15 and 16. In this way, in Fig. 2, we show a plot of $\log \omega$ vs $1000/T$. An activation

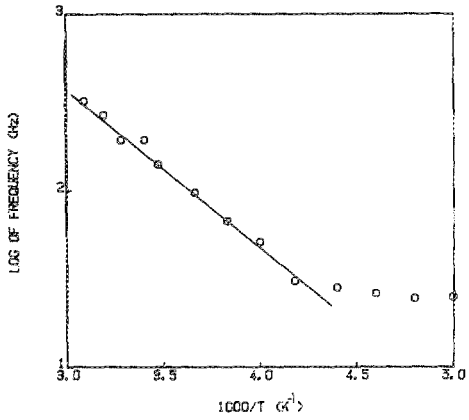


FIG. 2. Log of characteristic relaxation frequency vs $1000/T$ for the type 1 heterojunction.

energy of 80 meV can be deduced from the slope of the resulting straight line. This level, responsible for the relaxing behavior, is probably the 80-meV donor level which has been reported by many authors[17,18] associated with 6 Se vacancies.

Acceptor levels 80 meV above the valence band edge can be discarded because they would not cross the Fermi level, which is about 0.15 eV above the valence band. In any case, to our knowledge, no acceptor levels have been reported at such energetic depths.

The small peak observed in losses, at frequencies around $10^2$ Hz, did not show any temperature dependence. This could be explained in terms of the presence of interface states crossing the Fermi level. The very low intensity of the peak points to a very small quantity of those interface states. This will be discussed in detail in the following paragraph.

### 2. Type 2 heterojunctions

Figure 3 shows the results of *C-F* measurements of the representative type 2 cell (made of low-resistivity $10–10^{-1}$ $\Omega$ cm Cu-rich $CuInSe_2$) at 300 K. A relaxation is observed around $10^3$ Hz with no evidence for the presence of the $10^5$-Hz relaxation observed in the type 1 cell (see Fig. 1). Measurements at variable temperatures did not show measurable thermal activation in the characteristic frequency.

The temperature insensitivity of the relaxation located

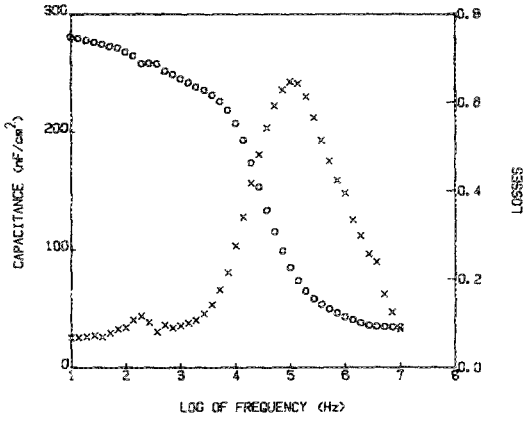


FIG. 1. Capacitance (O) and losses (×) vs frequency for the type 1 heterojunction, at 0-V dc bias and 300 K.

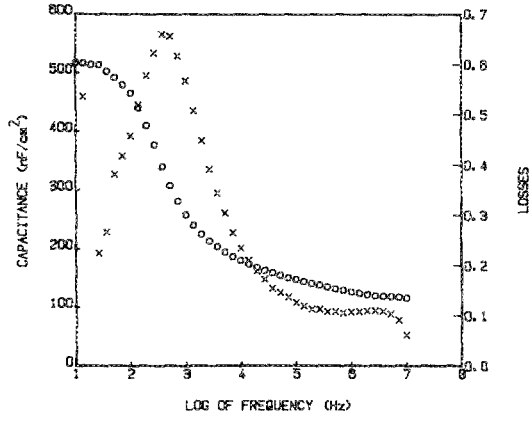


FIG. 3. Capacitance (O) and losses (×) vs frequency for the type 2 heterojunction, at 0-V dc bias and 300 K.

at $10^3$ Hz, together with the fact that the conduction mechanism was dominated by a high density of interface states,[10] leads us to associate that relaxation to the interface states. In the presence of high densities of interface states, the deionization of the level that interacts with the Fermi level will take place involving a great quantity of other levels and will perhaps take place by tunneling rather than by the usual thermal emission, thus justifying the lack of temperature dependence of the relaxation. In this way, the frequency dispersion of the capacitance can be associated with the presence of interface states.[19]

*C-F* measurements at forward dc bias voltages have also been performed on both types of cells. A relaxation appeared in both cells around $10^2$ Hz. The results obtained at 0.2 dc volts on the type 1 cell is depicted in Fig. 4. No temperature dependence again suggests that this behavior is due to the freeze-out of trapping and detrapping phenomena of interface states acting as recombination centers. When a forward bias is applied to the heterojunctions, the occupancy of the interface states will follow the variation of the bias voltage across the depletion region. The small alternating signal will then cause changes in the interface states density at the Fermi level if it can respond to the frequency of the applied signal. The capacitance can therefore be expressed as the sum of the depletion region capacitance and the contribution of the interface states[4,11] according to the following expression:

$$C = C_d + \{C_{is}/[1 + (\omega\tau)^2]\}, \tag{2}$$

where $C_d$ is the capacitance of the depletion region and contains the contribution due to deep levels, $C_{is}$ is the contribution to the capacitance due to interface states, and $\tau$ is the characteristic time of the relaxation process associated to interface states. Taking the simplest approach, the interface states at a frequency at which those levels can respond can be related to interface state densities at the Fermi level $N_{is}(V)$ (Refs. 11 and 20) according to the expression

$$N_{is}(V) = C_{is}(V)/q. \tag{3}$$

Capacitance measurements at forward bias can then be used to obtain information about the distribution of interface states. In Fig. 5 the relative distribution of interface states for both types of heterojunctions is shown. It can be useful to compare the density of such interface states in the vicinity of $V_{oc}$ (0.25 V) considering that the maximum power generation takes place at voltages near $V_{oc}$. Near-stoichiometric $CuInSe_2$ cells (type 1) showed interface states density in the range $10^{10}$–$10^{11}$ $cm^{-2}$ $eV^{-1}$, while Cu-rich cells (type 2) showed interface state density in the range $10^{12}$–$10^{13}$ $cm^{-2}$ $eV^{-1}$. The lack of photovoltaic response in those cells seems to be associated with the high density of interface states, probably related with a Cu excess at the interface. Cu-rich $CuInSe_2$ is known to originate Cu nodules at the interface[21] with CdS which destroy the photovoltaic response. Excess Cu will then very likely diffuse into the CdS during growth or post-deposition annealing, giving rise to an intrinsic CdS layer similar to that observed in $Cu_xS$/CdS cells, with a large density of extended interface states which justify a tunneling conduction mechanism observed in those cells.[19] This has been confirmed by *C-V* characteristics, as will be discussed later.

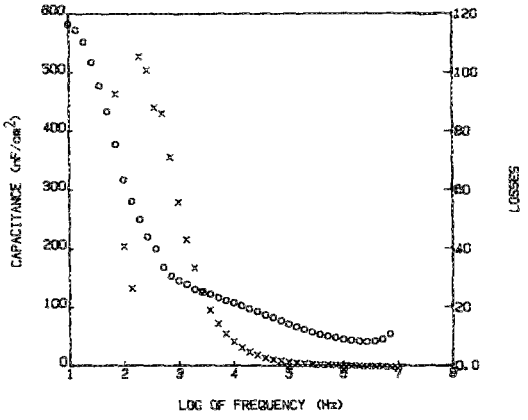


FIG. 4. Capacitance (O) and losses (×) frequency for the type 1 heterojunction, at 0.2-V dc forward bias and 300 K.

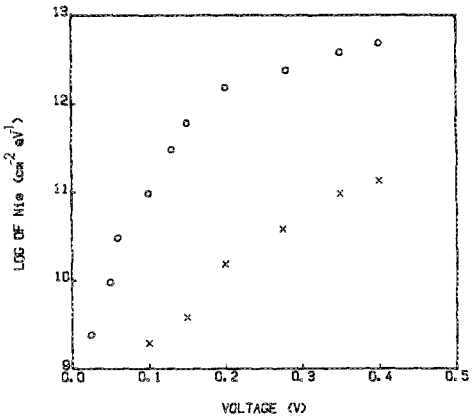


FIG. 5. Interface states distribution vs forward voltage for the type 1 (×) and the type 2 (O) heterojunctions.

### B. *C-V* measurements

When an ideal *p-n* junction is considered, the slope of a plot of the $C^{-2}$ vs V relationship for back-bias voltages is immediately related to the doping concentrations of the semiconductors at the edge of the depletion region. The extrapolated intercepts on the voltage axis can be used to find the built-in potential. In the presence of deep levels and interface states, the shape of the *C-V* relationship will be severely influenced by those states[20,22] and a more careful analysis is needed to obtain information from the *C-V* plots.

#### 1. Type 1 heterojunction

Figure 6 shows $1/C^2$ vs $V$ plots for the type 1 cell at 10 kHz [Fig. 6(a)] and at 5 MHz [Fig. 6(b)]. At 10 kHz, trapping and detrapping processes at the 80-meV donor level, quoted in the previous paragraph, can follow the ac signal, while the 5-MHz frequency is well beyond the relaxation frequency of that level. The increase in the capacitance observed at low forward bias voltages, Fig. 6(a), arises from the fact that the 80-meV donor level ceases crossing the Fermi level, as predicted by Roberts and Crowell.[22] The $1/C^2$ vs $V$ characteristic at 5 MHz, although it is taken at a frequency

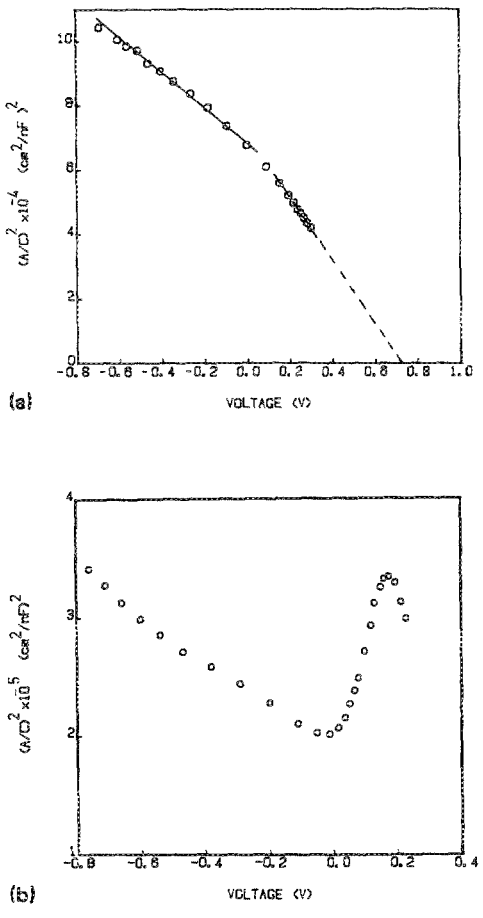


FIG. 6. (a) $1/C^2$ vs $V$ characteristic for the type 1 heterojunction, at 10 kHz and 300 K. (b) $1/C^2$ vs $V$ characteristic for the type 1 heterojunction, at 5 MHz and 300 K. Theoretical model (—) and experimental points (○).

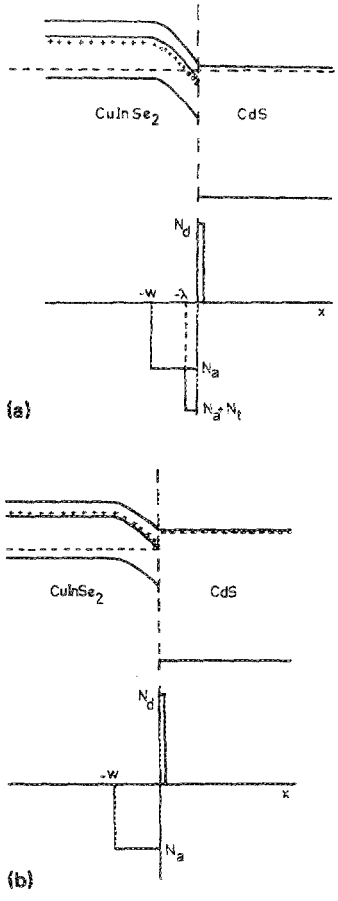


FIG. 7. (a) Band diagram and space-charge model for the type 1 heterojunction at reverse and 0-V polarization. (b) band diagram and space-charge model for the type 1 heterojunction at forward polarization.

at which the 80-meV donor level cannot respond, is also influenced by the deep level, as we will show in the following paragraphs.

Assuming that the built-in potential drops mainly in the $CuInSe_2$ layer, according to the differences in the doping concentrations, the simple model for the space-charge region depicted in Fig. 7 explains qualitatively the $1/C^2$ vs $V$ plot at high frequency.

At zero or reverse dc bias voltages [Fig. 7(a)], the donor level crosses the Fermi level, and an enhancement of the space-charge density is obtained (lower slope of the $1/C^2$ vs $V$ characteristic). At forward bias voltages [Fig. 7(b)], at which the donor level no longer crosses the Fermi level, the nonuniformity in the space-charge density disappears (higher slope of the $1/C^2$ vs $V$ characteristic) and an ideal case is achieved.

This simply space-charge models can be used to account for the experimental results according to the following calculations:

The slope of the $1/C^2$ vs $V$ characteristics at reverse or zero voltages (at which the donor level crosses the Fermi level) can be easily calculated.

Integrating Poisson equation, taking into account the boundary conditions one can write

$$V_D - V = \frac{q}{\epsilon}\left(\int_{-w}^{-w+\lambda} N_A x\,dx + \int_{-w+\lambda}^{0} (N_A + N_T)x\,dx\right), \tag{4}$$

where $V_D$ is the built-in potential, $w$ is the width of the depletion region, $\lambda$ is the width of the region for which the donor level is ionized, $N_A$ is the doping concentration of the $CuInSe_2$ film, and $N_T$ is the charge density at the 80-meV donor level. At sufficiently high frequencies, that the 80-meV donor level cannot respond, the capacitance per unit area can be written in the form

$$C = \epsilon/W. \tag{5}$$

The slope of the $1/C^2$ vs $V$ characteristic can be written applying Chain's rule:

$$\frac{\Delta 1/C^2}{\Delta V} = \frac{\Delta 1/C^2}{\Delta W}\left(\frac{\Delta(V_0 - V)}{\Delta W}\right) = \frac{2}{q\epsilon}\frac{1}{N_A + N_T(1 - \lambda/W)}, \tag{6}$$

so that the apparent carrier density deduced from the slope will be

$$N_{ap} = N_A + N_T[1 - (\lambda/W)]. \tag{7}$$

All the parameters of this expression can be calculated separately as follows:

(i) $N_A$ can be deduced from resistivity and mobility measurements resulting from $N_A = 1.5\times10^{16}$ cm$^{-3}$, as mentioned in Sec. II.

(ii) The number of trapping centers $N_T$ can be calculated using the change in capacitance ($\Delta C$) in the relaxation associated with the trap level; the room-temperature carrier concentration $N_A$ and the junction built-in voltage according to the model proposed by Pautrat *et al.*[23] The resulting value for $N_T$ was $1.8\times10^{17}$ cm$^{-3}$.

(iii) $\lambda$ can be obtained by integrating the electric field in the region calculated applying Gauss law. In this way, an expression for $\lambda$ results:

$$\lambda=\left(\frac{2\epsilon(E_t-E_f)}{q^2N_A}\right)^{1/2}, \tag{8}$$

where $E_t-E_f$ is the energetic distance between the 80-meV donor level and the Fermi level. A value of 200 Å results for $\lambda$.

(iv) $W$ is obtained from the high-frequency capacitance, according to expression (5), to be 2360 Å.

A vaue of $3.1\times10^{16}$ cm$^{-3}$ results for $N_{ap}$, in good agreement with the value deduced from the slope of the $1/C^2$ vs $V$ characteristics, that is, $3.3\times10^{16}$ cm$^{-3}$.

At forward bias voltages, when Fermi level no longer crosses the 80-meV donor level, the slope can be used in order to calculate the doping concentration in the $CuInSe_2$ side with no influence of such level, as quoted in the preceding paragraph. A value of $N_A=1.6\times10^{16}$ cm$^{-3}$, is achieved in very good agreement with that measured on the films with resistivity and Hall-effect measurements ($1.5\times10^{16}$ cm$^{-3}$, as quoted above). The built-in potential can now be deduced from the voltage axis intercept of the $1/C^2$ vs $V$ characteristic. A value of 0.75 V is obtained, in very good agreement with the theoretical predictions found for this parameter.[24]

In Fig. 6(a), theoretical predictions according to the simple theoretical model quoted above (straight line), and experimental data (points), can be observed. Agreement between both of them is excellent.

In the previous discussion, we did not take into account the presence of interface states, due to their low density, shown in Sec. III A. ($10^{10}$–$10^{11}$ cm$^{-2}$ eV$^{-1}$). Interface states, according to the model proposed by Ahrenkiel,[6] would have influenced the apparent built-in voltage, and not the doping densities, deduced from the slopes of the $1/C^2$ vs $V$ characteristics. Nevertheless, an easy calculation can be performed to show that their effect on the built-in voltage is negligible. Assuming, according to Ahrenkiel,[6] a change in the extrapolated intercept of the $1/C^2$ vs $V$ characteristic at $(1/C^2)=0$, due to interface states of

$$\Delta V=q\sigma_{ss}^2/2\epsilon N_D, \tag{9}$$

where $\sigma_{ss}$ is the density of interface states, deduced to be $10^{10}$–$10^{11}$ cm$^{-2}$ eV$^{-1}$ for type 1 heterojunctions in the preceding section, and taking for $N_D$ doping density a value of $9\times10^{17}$ cm$^{-3}$ (deduced from resistivity and Hall-effect measurements in CdS), values in the range $1.1\times10^{-5}$–$1.1\times10^{-3}$ V are deduced for $\Delta V$, obviously a negligible contribution to the 0.75 V value of the built-in voltage quoted above.

### 2. Type 2 heterojunction

Figure 8 shows $1/C^2$ vs $V$ plots for the type 2 heterojunction at 10 kHz [Fig. 8(a)] and at 5 MHz [Fig. 8(b)]. The increase of capacitance observed at 10 kHz at forward bias voltages can be explained in terms of the contribution to the capacitance due to interface states (as discussed above). The 5-MHz frequency is well beyond the characteristic frequency associated with trapping phenomena at interface states; therefore, this plot should be used to obtain information about doping profiles. The low slope of the $1/C^2$ vs $V$ plot, and the very high extrapolated intercept at the voltage axis (4.5 V), can be explained only in terms of an intrinsic zone in the space-charge region[25] in the CdS side, as we will show in the following paragraph.

The origin of that intrinsic region should be related to the fact that $CuInSe_2$ is Cu-rich, and this Cu excess tends to diffuse into the CdS side originating an intrinsic CdS layer, as we have discussed in Sec. III A. Assuming a space-charge density like that depicted in Fig. 9, the model proposed by Ahrenkiel[6] predicts an expression for $1/C^2$ that takes the form:

$$\frac{1}{C^2}=\frac{2}{q\epsilon N_D}\left((V_D-V)+\frac{q}{2\epsilon}N_D W^2-\frac{q\sigma_{ss}}{2\epsilon N_D}\right), \tag{10}$$

where $\sigma_{ss}$ is the interface states surface density and $W$ is the width of the depletion region in the CdS side.

An extrapolated intercept of the $1/C^2$ vs $V$ plot with the voltage axis of

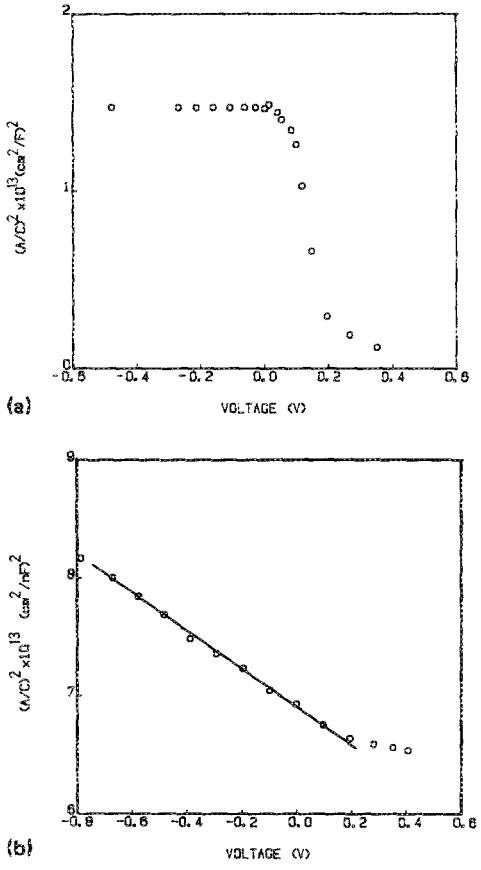


FIG. 8. (a) $1/C^2$ vs $V$ characteristic for the type 2 heterojunction, at 10 kHz. (b) $1/C^2$ vs $V$ characteristic for the type 2 heterojunction, at 5 MHz.

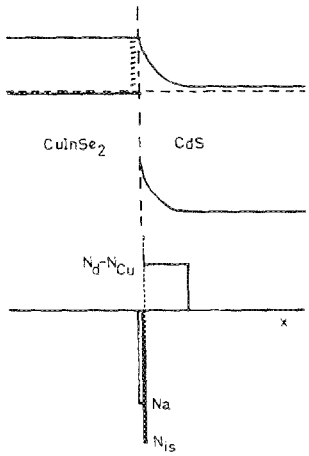


FIG. 9. Band diagram and space-charge model for the type 2 heterojunction.

$$V_D + \frac{q}{2\epsilon} N_D W^2 - \frac{q\sigma_{ss}}{2\epsilon N_D}$$

is predicted.

Taking $N_D = 9\times 10^{17}$ cm$^{-3}$, deduced from resistivity and mobility on our CdS films (see Sec. II) and assuming a tentative value for $W$, the value deduced for the width of the space-charge region from the high-frequency capacitance, a value for the intercept of 4.35 V is deduced in very good agreement with the value of 4.5 V measured experimentally, as quoted above.

On the other hand, doping density of $8\times 10^{17}$ cm$^{-3}$ is deduced for the CdS layer from the slope of the $1/C^2$ vs $V$ characteristic, also in very good agreement with the experimental value of $9\times 10^{17}$ cm$^{-3}$ quoted above.

We have shown that, assuming the existence of intrinsic region, the theoretical model proposed by Ahrenkiel[6] can be applied which accounts very well for our experimental results.

## IV. CONCLUSIONS

All-sputtered $CuInSe_2$/CdS solar cells heterojunctions have been analyzed. Depending on $CuInSe_2$ composition, two kinds of heterojunctions can be distinguished: type 1, based on stoichiometric or slightly In-rich chalcopyrite $CuInSe_2$ layers, and type 2 heterojunctions, based on Cu-rich chalcopyrite $CuInSe_2$ layers. Capacitance measurements have been used to study the effect of deep levels and interface states in the heterojunction characteristics.

Admittance spectroscopy measurements have shown the presence of a donor level in type 1 heterojunctions, located 80 meV below conduction band edge. $C$-$F$ measurements at forward bias permitted us to obtain a relative distribution of interface states in both kinds of heterojunctions. Values in the range $10^{10}$–$10^{11}$ cm$^{-2}$ eV$^{-1}$ have been found in type 1 heterojunctions; and values in the range $10^{12}$–$10^{13}$ cm$^{-2}$ eV$^{-1}$ in type 2 heterojunctions.

$C$-$V$ measurements were used to obtain information about the electronic structure of the space-charge region in both kinds of heterojunctions. In type 1 heterojunctions, a two-slope $1/C^2$ vs $V$ characteristic is found as a consequence of the uncovered charge in the 80-meV donor level. A simple theoretical model is developed to obtain doping concentration in the $CuInSe_2$ layer and trapped charge in the 80-meV donor level.

In type 2 heterojunctions, the flat $1/C^2$ vs $V$ characteristic is interpreted in terms of the presence of an intrinsic layer in the CdS side, as a consequence of Cu diffused from the Cu-rich $CuInSe_2$ layer. According to the model proposed by Ahrenkiel,[6] doping concentration for the CdS can be found from the slope of the $1/C^2$ vs $V$ characteristic. Calculated values were in very good agreement with those deduced from resistivity and Hall-effect measurements performed on the CdS films.

## ACKNOWLEDGMENT

This work was partially financed by the Spain-USA Joint Committe under Grant No. CCA-8411046.

[1] M. N. Ruberto and A. Rathwarf, J. Appl. Phys. **6**, 4662 (1987).
[2] R. K. Ahrenkiel, J. Appl. Phys. **59**, 181 (1986).
[3] M. Eron and A. Rothwarf, J. Appl. Phys. **57**, 2275 (1985).
[4] H. Tavakolian and J. R. Sites, in *Proceedings of the 18th IEEE Photovoltaic Specialists' Conference*, Las Vegas, NV, 1985 (IEEE, New York, 1986), p. 1065.
[5] V. Ramanathan, R. Noufi, and R. C. Powell, J. Appl. Phys. **63**, 1203 (1988).
[6] R. K. Ahrenkiel, Sol. Cells **16**, 549 (1986).
[7] D. L. Losse, J. Appl. Phys. **46**, 2204 (1975).
[8] I. Martil, G. Gonzalez-Diaz, and F. Sanchez-Quesada, Thin Solid Films **114**, 327 (1984).
[9] I. Martil, J. Santamaria, E. Iborra, G. Gonzalez-Diaz, and F. Sanchez-Quesada, J. Appl. Phys. **62**, 4163 (1987).
[10] J. Santamaria, I. Martil, E. Iborra, G. Gonzalez-Diaz, and F. Sanchez-Quesada (unpublished).
[11] H. Tavakolian and R. E. Hollingsworth, J. Vac. Sci. Technol. A **4**, 488 (1986).
[12] K. L. Chopra and S. R. Das, *Thin Film Solar Cells* (Plenum, New York, 1983).
[13] L. B. Fabrick and K. L. Eskenas, in *Proceedings of the 18th IEEE Photovoltaic Specialists' Conference*, Las Vegas, NV, 1985 (IEEE, New York, 1986), p. 754.
[14] L. C. Isset, J. Appl. Phys. **56**, 3508 (1984).
[15] D. V. Lang, J. D. Cohen, and J. P. Harbison, Phys. Rev. B **25**, 5285 (1982).
[16] A. K. Jonscher, *Dielectric Relaxation in Solids* (Chelsea Dielectric, London, 1983).
[17] C. Rincon, C. Bellabarba, J. Gonzalez, and G. Sanchez-Perez, Sol. Cells **16**, 335 (1986).
[18] G. Masse and E. Redjai, J. Appl. Phys. **56**, 1154 (1984).
[19] J. Santamaria, E. Iborra, I. Martil, G. Gonzalez-Diaz, and F. Sanchez-Quesada, Semicond. Sci. Technol. **3**, 781 (1988).
[20] L. C. Kimmerling, J. Appl. Phys. **45**, 1839 (1974).
[21] T. J. Coutts and J. D. Meakin, Eds., *Current Topics in Photovoltaics* (Academic, London 1986).
[22] G. I. Roberts and C. R. Crowell, J. Appl. Phys. **41** 1767 (1970).
[23] J. L. Pautrat, B. Katircioglu, N. Magnea, D. Bensahel, J. C. Pfister, and L. Revoil, Solid State Electron. **23**, 1159 (1980).
[24] A. Rothwarf, Sol. Cells **16**, 567 (1986).
[25] R. B. Hall and V. P. Singh, J. Appl. Phys. **50**, 6406 (1979).